Appl Phys A (2010) 98: 861–865
DOI 10.1007/s00339-010-5553-z

Applied Physics A
Materials Science & Processing

Giant magnetoimpedance effect and voltage response in meander shape Co-based ribbon

Lei Chen · Yong Zhou · Chong Lei · Zhi-Min Zhou

Received: 4 August 2009 / Accepted: 8 January 2010 / Published online: 27 January 2010

Abstract Field-annealed Co-based amorphous ribbon (Metglas® 2705M) with a meander structure is fabricated by MEMS technology and the giant magnetoimpedance (GMI) effects are studied at different magnetic fields and frequencies. The maximum longitudinal GMI ratio of the ribbon is 193.7% and the magnetic field sensitivity is 17.4%/Oe. The maximum GMI ratio of the meander ribbon is much larger than the single strip ribbon mainly due to the larger change ratio of inductance L. The sensitivity of an output U reach up to 10 V/A and U thermal fluctuation is less than 15 mV in the temperature range of −20 to 40°C. This meander shape ribbon can be considered as a good candidate for the GMI-based sensor fabrication.

1 Introduction

The giant magnetoimpedance (GMI) effect is the change of the impedance experienced by an AC current flowing through a magnetic material when an external DC magnetic field is applied. This effect has been extensively studied in soft amorphous ferromagnetic wires [1–5], thin films [6–9], and ribbon [10–13] in last decade for their potential applications in magnetic field sensing [14], material nondestructive evaluation [15], and biosensing [16–18]. Co-based amorphous ribbon has been studied for many years in order to improve its soft magnetic properties [19–21]. It exhibits the GMI effect which may be related to the high transverse permeability caused by the transversely oriented domain configuration [22]. The ribbon has low magnetostriction and the magnetic anisotropy can be easily controlled. Consequently, much effort has been done in enhancing the GMI performance and practicality of Co-based amorphous ribbon in recent years [16, 18, 23–26]. Sensor applications require the stability and the sensitivity of the GMI response to the external magnetic field combined with the smallest size of the samples; therefore it is the best choice to use MEMS technology to fabricate the sensor. Recently, Zhou [27] reveals that the GMI response in the NiFe thin film with a meander structure has a great improvement compared with a single-strip sample. However, less reports is presented on the GMI effect in Co-based amorphous ribbon with a meander structure.

The aim of this work is to investigate the GMI performance of a micropatterned Co-based ribbon and the enhanced GMI effect in a meander-structure ribbon. The field-annealed Co-based ribbon (Metglas® 2705M) with a meander structure is fabricated by the MEMS technology. The longitudinal GMI effect in this ribbon is investigated at various frequencies. The results are compared with the GMI response in the ribbon with single-strip structure and the differences between them are discussed. The output voltage U to the measuring current I is tested in the temperature range of −20–40°C to verify the sensitivity and the stability of the patterned ribbon.

2 Experimental details

The samples with a meander shape are made of Co-based commercial amorphous ribbon (Metglas® 2705M) with

L. Chen (✉) · Y. Zhou · C. Lei · Z.-M. Zhou
National Key Laboratory of Nano/Micro Fabrication Technology, Key Laboratory for Thin Film and Microfabrication of Ministry of Education, Institute of Micro/Nano Science and Technology, Shanghai Jiao Tong University, Dong Chuan Road 800, Shanghai 200240, China
e-mail: leon_chen@sjtu.edu.cn

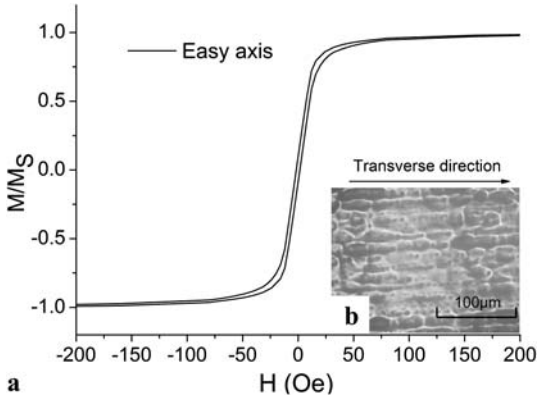

Fig. 1 (**a**) The magnetization curve and (**b**) transverse domain structure of the field-annealed ribbon. External field applied along the transverse direction of ribbon (easy axis) during the magnetization curve measurement

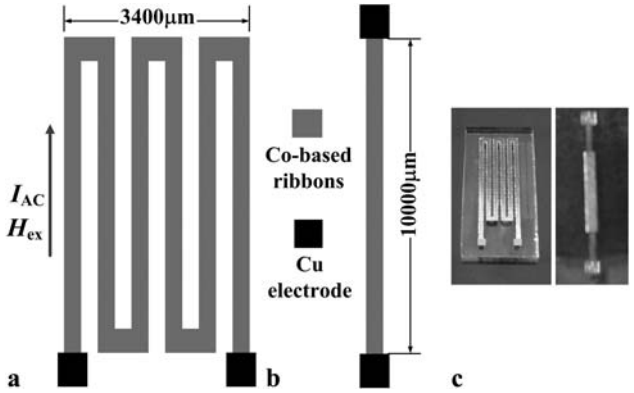

Fig. 2 Top view of the micro-patterned ribbon with (**a**) meander structure and (**b**) single strip structure; (**c**) photograph of the samples

30 μm in thickness, and the physical properties of this ribbon are as follows: the max permeability μ_{max} is 6×10^5, the resistivity ρ is 136 μΩ cm, the saturation magnetostriction ≪1 ppm, and the Curie temperature is 365°C. Before fabricating process, the ribbon is subjected to annealing treatment at 380°C (slightly higher than Curie temperature) with a transverse magnetic field in vacuum to induce transverse anisotropy. The annealing system has a small vacuum chamber within which the ribbon can be fixed firmly and the chamber can be evacuated down to a base pressure of 0.3 Pa. The chamber is placed into the center of a pair of Helmholtz coil and the field strength of 16 kA/m (nearly saturation magnetization) is generated along the transverse direction of ribbon. The transversal induced anisotropy is evident from the magnetization curve as shown in Fig. 1a and the domain structure of the ribbon in Fig. 1b. The field distribution is sharp and symmetric. The hysteresis loop of the field-annealed ribbon shows nearly null coercivity and remanence. The domain structure of annealed sample shows the uniform transverse anisotropy.

The micropatterned ribbon is fabricated by photolithography, chemical etching, and electroplating methods. After bonding the ribbon on glass substrates using an epoxy adhesive, the photoresistive layer with a thickness of 10 μm is coated on the ribbon layer and exposed. The ribbon is etched in an acidic solution (mixture of HNO_3, HCl, and H_2O with a certain proportion) for about ten minutes. As chemical etching is an isotropic process, a certain amount of undercutting and profile roughness is expected. The photomasks give 420-μm line width to photoresistive layer to compensate the undercutting. After etching process, the line width of the single-strip structure and of each segment of a meander structure is measured by a profiler and the width is 400 ± 2 μm. The space between adjacent longitudinal straight lines of meander ribbon is 200 ± 2 μm. With the comparatively large size of the meander structure, the error of 2 μm is considered to be acceptable. Cr/Cu seed layer with a thickness of 100 nm is deposited on a patterned ribbon and a substrate by RF sputtering. Then the 0.5 mm × 0.5 mm Cu electrodes with a thickness of 20 μm are electroplated. After the photoresistive layer is removed, the seed layer that beyond the patterned structure is removed by reactive iron etching method. Finally, the total dimension of the meander shape ribbon is 3400 μm (width) × 10000 μm (length) and the meander structure with three turns is shown in Figs. 2a and 2c. In addition, the magnetization curve of an etched ribbon is also measured to observe the influence of the etched treatment on the anisotropy of the ribbon; the result shows that the difference between before and after etch treatment are very small and can be nearly ignored. It may be related to the fact that the sample studied here is annealed in a relatively large magnetic field of 200 Oe.

The GMI effects are measured by an impedance analyzer (HP4194A). The AC current that flow through the ribbon with the constant amplitude of 10 mA and with the frequency in the range of 0.1–40 MHz. An external magnetic field (H_{ex}) of 1–150 Oe is applied along the longitudinal direction (perpendicular to easy axis). Figure 1a shows the direction of the AC current and the external magnetic field. Due to limitations of our experimental device to reach saturation field for samples, the GMI ratio is calculated from $Z(H)$ curves defined as: GMI ratio $= 100\% \times [Z(H) - Z(H_{max})]/Z(H_{max})$, where $Z(H_{max})$ is the magnetoimpedance with a 150-Oe magnetic field applied.

3 Results and discussion

In the frequency range of 1–40 MHz, the field characteristics of a GMI in a meander ribbon for the longitudinal field exhibit sharp change at around 10 Oe, as can be seen in Fig. 3. The maximum GMI ratio is 193.7% at the magnetic field $H_{ex} = 10$ Oe and the frequency $f = 20$ MHz.

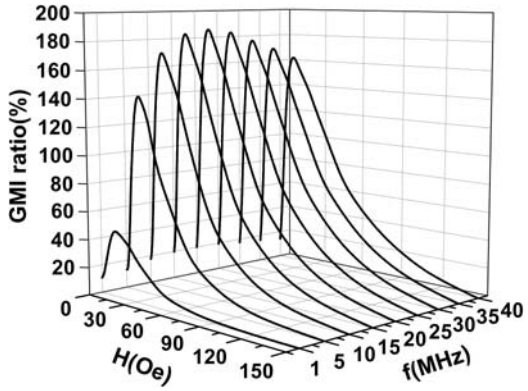

Fig. 3 Field dependences of longitudinal GMI effect in meander shape ribbon at different frequency

With the increase of the applied magnetic field, the magnitude of the GMI ratio is reaching a sharp peak and then gradually decreases to zero [6]. It is a typical characteristic of longitudinal GMI spectra of the soft magnetic materials with a high-transverse permeability. All of the curves in Fig. 2 are in good agreement with this characteristic. This phenomenon can be explained by the magnetization rotation model [22] at high frequency in which the transversal magnetic permeability increases with the increasing magnetic field and reaches a maximum value at $H_L = H_K$ (H_K is the anisotropy field of samples). In the linear range of 2–10 Oe, the GMI field sensitivity is 17.4%/Oe at 20 MHz. In the range of 0–20 MHz, the GMI peak value of patterned ribbon increases with frequency and reaches its maximum. It should be noted that the GMI effect increases with frequency because the impedance is proportional to $(\omega\mu_T)^{1/2}$, here $f = \omega/2\pi$ is the frequency of the AC current and μ_T is the transverse permeability, but in the case of decreasing transverse permeability at higher frequencies, this trend becomes not obvious.

The calculated impedance Z of a planar ribbon based on the classical skin effect solution of the reduced Maxwell equation is [22, 28]

$$Z = R_{\mathrm{dc}} \cdot \mathrm{j}ka \coth(\mathrm{j}ka) \tag{1}$$

where $2a$ is the thickness of the ribbon, R_{dc} is the electrical resistance for a DC current, and $k = (1 + \mathrm{j})/\delta_m$ with imaginary unit j. δ_m is the skin depth in the ribbon with a transverse permeability μ_T,

$$\delta_m = \frac{c}{\sqrt{4\pi^2 f \sigma \mu_T}} \tag{2}$$

where c is the speed of light and σ is the electrical conductivity. According to (1) and (2), GMI can be understood as the consequence of the increase of the skin depth until it reaches half the thickness of the ribbon through the decrease of the transverse permeability in (2) under an external magnetic field. In order to get a larger GMI effect, it is necessary to reduce skin depth by choosing magnetic materials that have large permeability μ and small δ_m and R_{dc}. Moreover, although the relatively high GMI ratio is obtained from the meander structure, this structure has inhomogeneous magnetic structure; further research work should be carried out to investigate the asymmetric GMI effect and the GMI hysteresis in this structure.

Next, in order to understand the influence of the meander structure on the GMI effect, the comparison of impedance Z, resistance R, and reactance X between the meander and the single-strip structure at 20 MHz is carried out. The single strip structure ribbon has the same length (10000 μm) and line width (400 μm) as the meander structure (shown in Fig. 2c). As it is well known, Z is consists of its real part R and imaginary part X, the combined action of R and X lead to the change of Z. It is obviously shown in Fig. 4 that the GMI ratio in meander structure is larger than in the single strip. In a single-strip ribbon, field dependence of X is a flat curve, only R plays a major contribution to the change of Z. But in the meander structure, X begins to make big contribution to the change of Z together with R. With respect to the relationship between X and inductance L is $X = \omega L$, the formula of Z, R, X, and L can be expressed as follows [29]:

$$\begin{aligned} Z(\omega, \mu_T) &= R(\omega, \mu_T) + \mathrm{j}X(\omega, \mu_T) \\ &= R(\omega, \mu_T) + \mathrm{j}\omega L(\omega, \mu_T) \\ &= \frac{\rho l}{2w\delta} + \mathrm{j}\omega L(\omega, \mu_T), \end{aligned} \tag{3}$$

where ρ is the resistivity of ribbon, l is the total length of patterned ribbon, and w is the line width of the ribbon, respectively. According to this formula, the enhanced GMI effect in meander structure can be explained from the larger change ratio of X and L.

When an AC current flows through the meander structure, just as a plane inductance, the magnetic flux in the longitudinal straight lines will correlate each other by mutual inductance of magnetic chain. Due to this mutual inductance effect, the change ratio for inductance of meander structure is bigger than the single-strip structure under the same changes of magnetic field. Because of the relationship between Z and L, $Z = R + \mathrm{j}\omega L$, this meander structure will lead to a larger change ratio of Z and thus lead to a larger GMI effect. For a ferromagnetic conductor, it is a comparatively complicated process to calculate the mutual inductance of a meander conductor because several factors should be considered, such as the distribution of the magnetic field in a conductor and an exterior space, the distribution of an AC current, the magnetic interaction among each individual line segments, the effect of the domain structure, and the magnetoelastic anisotropies on a permeability, and so on. But it can

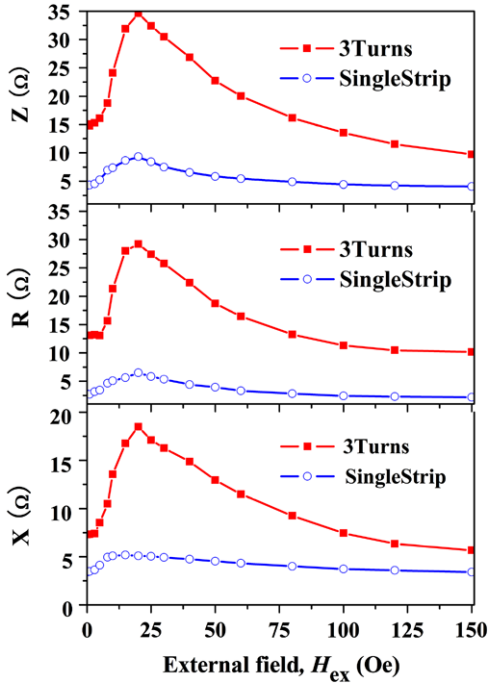

Fig. 4 Field dependence of Z, R and X of the ribbon with different structure at the frequency of 20 MHz: meander and single strip structure

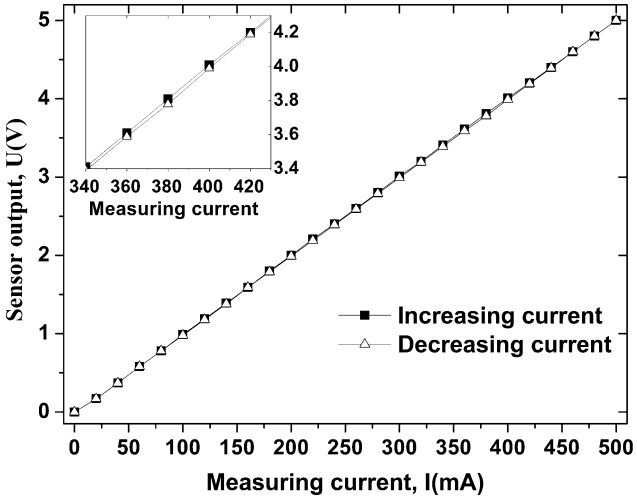

Fig. 5 DC voltage response of the meander ribbon versus the measuring current at the bias field of 10 Oe

be confirmed that the mutual inductance of the ribbon with a meander structure has big contribution to the GMI effect, and the more turns of the meander structure is, the bigger contribution becomes. Moreover, it can be observed from Fig. 4 that there is a slight enhancement of the anisotropy field when going from the single strip to the meander structure, and it can be ascribed to the inhomogeneous magnetic structure of the meander structure ribbon. It demonstrates the effect of structural change on an anisotropy field in a magnetic system.

In a view of the above GMI characteristics of the field-annealed ribbon with a meander structure, the bias magnetic field H_b of 10 Oe is applied to investigate the DC voltage response of the meander ribbon. Figure 5 shows that the ribbon final response U to the measuring current I in the range of 0–0.5 A, the sensitivity of U reach 10 V/A by adjusting the reference voltage. In the current range of 340–420 mA, an increasing and decreasing output voltage shows very small deviations maybe due to the Joule contribution in the ribbon that generated by the measuring current and the inhomogeneous magnetic structure of ribbon. Thermal noise is a very important issue in magnetic systems when we refer to the output fluctuation of the magnetic sensor. In order to measure the temperature stability of the voltage output of the ribbon, the output U is measured while the ribbon is heated and cooled. Also the voltage output of the ribbon is measured again at room temperature. To avoid the magnetostriction influence during heating and cooling, we fixed the sample on the substrate using a small mechanical fixture. Thermal fluctuation of U is less than 15 mV in a temperature range between −20 and 40°C. It is mainly due to the Johnson noise generated by the thermal agitation of the charge carriers in the ribbon and the thermal fluctuation noise from the ribbon to the Cu electrode.

The ribbon with a meander structure shows fairly good sensitivity and stability of the output voltage, and it also shows a relatively high GMI ratio. It is low cost and easier to fabricate when compared with other structures, such as multilayer thin film and wire. Thus it can be considered as a good candidate to fabricate the GMI-based sensor with good performance.

4 Conclusion

The longitudinal GMI effects in field-annealed Co-based ribbon with a meander structure are studied. The maximum longitudinal GMI ratio is 193.7% at $H_L = 10$ Oe and frequency $f = 20$ MHz. In the range of 0–10 Oe, the GMI field sensitivity is 17.4%/Oe at 20 MHz. The GMI effect in the meander structure is larger than in the single-strip structure due to the larger change ratio of inductance L during the GMI measurement. The ribbon with a meander structure also shows fairly good sensitivity and stability of the output voltage.

Acknowledgements The authors would like to thank the National High Technology Research and Development Program (2006AA03-Z301), the Nanotechnology Program of Shanghai Science & Technology committee (Nos. 0652nm004, 0752nm004), National Key Lab Research Fund (No. 9140C7903090707), the Non-Silicon Precision Micromachining & Microfabrication Technology (D2320060098), State Key Development Program of Basic Research of China (2010CB933901), and Basic Research Program of Science & Technology Committee of Shanghai (09JC1408600) for the support given in this work.

References

1. X.P. Li, Z.J. Zhao, C. Chua, H.L. Seet, L. Lu, J. Appl. Phys. **94**, 7626 (2003)
2. J.P. Sinnecker, M. Knobel, K.R. Pirota, J.M. Garcia, A. Asenjo, M. Vazquez, J. Appl. Phys. **87**, 4825 (2000)
3. F.E. Atalay, H. Kaya, S. Atalay, J. Phys. D, Appl. Phys. **39**, 431 (2006)
4. P. Ripka, *Magnetic Sensors and Magnetometers* (Artech House Publishers, Boston, 2001), pp. 350–359
5. L.V. Panina, K. Mohri, Appl. Phys. Lett. **65**, 1189 (1994)
6. R.L. Sommer, C.L. Chien, Appl. Phys. Lett. **47**, 3346 (1995)
7. T. Morikawa, Y. Nishibe, H. Yamadera, Y. Nonomura, M. Takeuchi, J. Sakata, IEEE Trans. Magn. **32**, 4965 (1996)
8. Y. Zhou, J.Q. Yu, X.L. Zhao, B.C. Cai, J. Appl. Phys. **89**, 1961 (2001)
9. D.P. Makhnovskiy, L.V. Panina, N. Fry, J. Mapps, J. Magn. Magn. Mater. **272–276**, 1866 (2004)
10. V.E. Makhotkina, B.P. Shurukhina, V.A. Lopatina, P.Yu. Marchukova, Yu.K. Levina, Sens. Acta A **25–27**, 759 (1991).
11. K.S. Byon, S.C. Yu, C.G. Kim, J. Appl. Phys. **89**, 7218 (2001)
12. M.H. Phan, H.X. Peng, M.R. Wisnom, S.C. Yu, N.H. Nghi, C.G. Kim, Sens. Acta A **129**, 62 (2006)
13. F. Alves, L. Abi Rached, J. Moutoussamy, C. Coillot, Sens. Acta A **142**, 459 (2008)
14. K. Tan, K. Yamakawa, T. Komakine, M. Yamaguchi, Y. Kayano, H. Inoue, J. Appl. Phys. **99**, 08B315 (2006)
15. I. Elshafiey, A. Mohra, J. Circuits, Syst. Comput. **16**, 847 (2007)
16. G.V. Kurlyandskaya, M.L. Sanchez, B. Hernando, V.M. Prida, P. Gorria, M. Tejedor, Appl. Phys. Lett. **82**, 3053 (2003)
17. H. Chiriac, M. Tibu, A.E. Moga, D.D. Herea, J. Magn. Magn. Mater. **293**, 671 (2005)
18. G.V. Kurlyandskaya, V.F. Miyar, A. Saad, E. Asua, J. Rodriguez, J. Appl. Phys. **101**, 054505 (2007)
19. R. Krishnan, K. LeDang, V.R.V. Ramanan, P. Veillet, J. Magn. Magn. Mater. **5457**, 263 (1986)
20. L. Fernandez-Barquin, J. Rodriguez-Fernandeza, J.C. Gomez-Sala, J. Magn. Magn. Mater. **83**, 357 (1990)
21. Y. Masaaki, S. Takao, IEEE Trans. Magn. **26**, 1409 (1990)
22. L.V. Panina, K. Mohri, T. Uchiyama, M. Noda, IEEE Trans. Magn. **31**, 1249 (1995)
23. A. Kumar, S. Mohapatra, V.F. Miyar, A. Cerdeira, J.A. Garcia, H. Srikanth, J. Gass, G.V. Kurlyandskaya, Appl. Phys. Lett. **91**, 143902 (2007)
24. P. Kollu, L. Jin, K.W. Kim, S.S. Yoon, C.G. Kim, Appl. Phys. A **90**, 533 (2008)
25. L. Chen, Y. Zhou, C. Lei, Z.M. Zhou, W. Ding, J. Phys. D, Appl. Phys. **42**, 145005 (2009)
26. L. Chen, Y. Zhou, Z.M. Zhou, W. Ding, Phys. Stat. Sol. A **206**, 1594 (2009)
27. Z.M. Zhou, Y. Zhou, Y. Cao, J. Magn. Magn. Mater. **320**, e967 (2008)
28. S.S. Yoon, S.C. Yu, G.H. Ryu, C.G. Kim, J. Appl. Phys. **85**, 5432 (1999)
29. C. Kittel, Phys. Rev. **70**, 281 (1946)